©2004 The Visualization Society of Japan and Ohmsha, Ltd.
Journal of Visualization, Vol. 7, No. 3 (2004) 187-199

A Visualization Study of Fluid-Structure Interaction between a Circular Cylinder and a Channel Bed

Rao, S. K.*[1], Sumner, D.*[1] and Balachandar, R.*[2]

*1 Department of Mechanical Engineering, University of Saskatchewan, 57 Campus Drive, Saskatoon, Saskatchewan, S7N 5A9, Canada.
E-mail: david.sumner@usask.ca
*2 Department of Civil and Environmental Engineering, University of Windsor, Essex Hall, 401 Sunset Avenue, Windsor, Ontario, N9B 3P4, Canada.

Received 13 February 2003
Revised 25 November 2003

***Abstract*:** Flow visualization was used to study the fluid-structure interaction between a circular cylinder and a shallow turbulent open channel flow. The Reynolds number ranged from Re_D = 1500–4400 based on the cylinder diameter, and from Re_H = 7,800–27,600 based on the channel hydraulic radius. The cylinder was mounted vertically on the channel bed and the flow depth-to-cylinder-diameter ratio was varied from d/D = 7.0–11.7. Tests were carried out over smooth and rough beds, with the rough beds being either permeable or impermeable. The study showed that the horseshoe vortex forming at the cylinder-bed junction affects many of the flow structures, including the mode of vortex shedding, the shear layer dynamics, the vortex formation length, and the width of the near-wake region. The influence of the horseshoe vortex can be recognized throughout the depth of flow; however, its influence decreases with an increase in distance from the channel bed. It was also possible to discern that the bed roughness resulted in a change to the above interaction and the permeability of the bed resulted in additional changes.

***Keywords*:** Cylinder, Open Channel Flow, Horseshoe Vortex, Vortex Shedding.

1. Introduction

A circular cylinder immersed in a uniform approach flow has been a well-studied problem in fluid mechanics (Sumer and Fredsoe, 1997). The flow field is characterized by the alternate, periodic shedding of Kármán vortices for a wide range of Reynolds number. In many practical applications a cylindrical structure interacts with a non-uniform approach flow, which may influence the vortex shedding behaviour and the hydrodynamic forces acting on it. An example is the case of a circular cylinder mounted normal to a channel bed (Fig. 1), which has received considerable attention because of its common occurrence in many practical problems, such as the flow around bridge pylons, piers, and offshore structures (Dargahi, 1989; Yulistiyanto et al., 1998; Rouland, 2000; Simpson, 2001; Kahraman et al., 2002). The horseshoe vortex that forms at the junction of the cylinder and the channel bed (or wall, depending on the application), where the wall boundary layer interacts with the flow around the cylinder, modifies the regular Kármán vortex shedding process and development of the cylinder wake. For an erodible, permeable channel bed, the horseshoe vortex may make additional contributions to the forces causing scour around the cylinder base (Ahmed and Rajaratnam, 1998; Dey, 1999; Istiarto and Graf, 2001). Scour can weaken the support of the structure

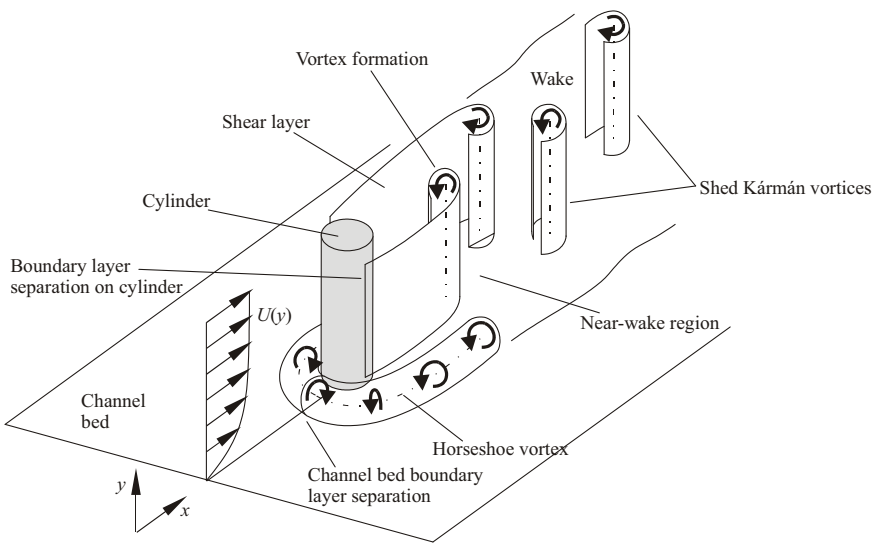

Fig. 1. Circular cylinder mounted normal to a channel bed.

and enhance the release into the flow of contaminants previously settled within and on the channel bed.

In shallow, turbulent open channel flows, where the streamwise length scales characterizing the flow are dominant (as opposed to the channel depth), the horseshoe vortex, the free surface, the depth of flow, and the roughness and permeability of the channel bed, will together have a strong influence on the flow around the cylinder. Although extensive literature exists on the effects of roughness (Grass, 1971; Krogstad and Antonia, 1994, 1999; Balachandar and Ramachandran, 1999; Tachie et al., 2000; Balachandar et al., 2001; Bergstrom et al., 2001), and to some extent permeability (Zagni and Smith, 1976; Zippe and Graf, 1983; Dasgupta and Paudyal, 1985; Mendoza and Zhou, 1993; Nikora et al., 2001; Rao, 2003), on the turbulent boundary layer parameters, there have been relatively few studies that have examined their effects on flow around the surface-mounted cylinder. An improved understanding of these effects will be useful in the development of drag reduction and scour prevention mechanisms, and in the areas of flow-induced vibrations, wake development, and mixing of streambed contaminants. In the present study, flow visualization experiments with a circular cylinder mounted on a channel bed (smooth, rough impermeable, and rough permeable) were undertaken to acquire new insight into the complex fluid-structure interaction involved with this flow.

2. Background

2.1 Open Channel Flows

In deep open channel flows, the horizontal length scale of a typical eddy is a small portion of the depth of the flow (French, 1985). However, in some developing and fully developed cases, the boundary layer occupies as much as 60% to 100% of the channel depth, and the horizontal length scales of the flow are significantly larger than the depth of the flow (Balachandar and Ramachandran, 1999). In these flows, bed friction becomes increasingly important (Ramachandran, 1999). In flows involving a rough bed, the effects of roughness are presently thought to pervade throughout most of the depth of flow; this aspect is now being further discussed and a body of literature is evolving on this topic (Krogstad and Antonia, 1994, 1999; Tachie et al., 2000; Balachandar et al., 2001; Bergstrom et al., 2001). The near-wall ejections are transported to the outer regions and hence these effects have been shown to be prevalent through most of the depth (Grass, 1971). This, along with the presence of a shear-free surface at the top, makes the shallow open channel flow more complex.

Further complexity arises when the effect of permeability is considered; its effect on the

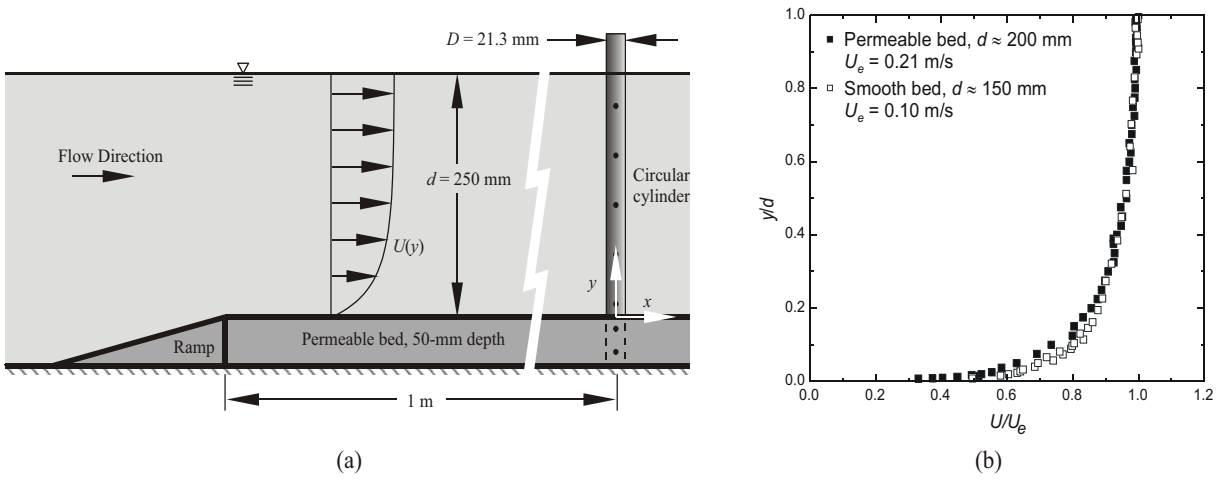

Fig. 2. Experimental set-up: (a) schematic (not to scale) of the hydraulic flume, showing the rough permeable sand bed, d = 250 mm; (b) examples of channel mean velocity profiles, from Rao (2003).

streamwise mean velocity has been discussed by Zagni and Smith (1976), Zippe and Graf (1983), Dasgupta and Paudyal (1985), Mendoza and Zhou (1993), and Nikora et al. (2001). Flow over a permeable bed involves complex interactions between the bed, the seepage flow and the main flow, where there is a continuous transfer of mass, momentum and energy between them. This in turn alters the way in which bed roughness affects the flow (Dasgupta and Paudyal, 1985) and results in the presence of a finite slip velocity. Also, the virtual origin of the mean velocity profile is displaced farther below the bed surface, and there is an increase in the coefficient of friction. Nikora et al. (2001) suggest the inclusion of a sub-surface layer, in addition to the outer layer, the log-layer and the roughness layer. The sub-surface layer occupies the pores below the roughness layer where the flow is driven by gravity and momentum fluxes from the overlying layers.

2.2 Circular Cylinder Normal to a Channel Bed

Many researchers have studied the case of an infinite circular cylinder of diameter, D, immersed in a uniform cross-flow, where flow separation and Kármán vortex shedding are considered primarily from a two-dimensional perspective (Sumer and Fredsoe, 1997). Elevated levels of freestream turbulence, the cylinder aspect ratio (depth/diameter ratio, d/D), end effects, axially sheared flow, proximity to a wall, and a shallow flow, all of which may encountered to varying degrees in practical applications, have pronounced effects on the cylinder flow field. The effects of elevated freestream turbulence are similar to an increase in the Reynolds number, which reduces the velocity at which the critical, post-critical and trans-critical regimes occur (Bearman and Morel, 1984; Norberg, 1986). The cylinder aspect ratio (d/D = 7.0–11.7 in the present study, and thus in the low-to-medium range) can affect the drag coefficient, vortex shedding frequency, and spanwise uniformity of the flow (Norberg, 1986; Szepessy and Bearman, 1992). Axial shear flow, as in the present study, can result in cellular vortex shedding, spanwise variation of the base pressure and sectional drag coefficient, and a lower critical Reynolds number (Griffin, 1985).

The flow around a surface-mounted circular cylinder (Fig. 1), where the axis of the cylinder is normal to the channel bed, is particularly complex (Dargahi, 1989; Rouland, 2000; Simpson, 2001; Kahraman et al., 2002). Here, the cylinder is immersed in a non-uniform approach flow, $U(y)$, and the local flow field about the cylinder-wall junction and along the span becomes strongly three-dimensional. The flow is characterized by a region of separated flow upstream of the cylinder at the cylinder-wall junction. From this region is formed the horseshoe vortex, which extends around the sides of the cylinder and into the wake. The horseshoe vortex has been studied in the context of scour (Dargahi, 1989; Rouland, 2000; Ahmed and Rajaratnam, 1998; Dey, 1999) and roughness effects (Rouland, 2000; Ahmed and Rajaratnam, 1998; Balachandar and Patel, 2002). In the region x/D < 8, the turbulent character of the wake is amplified and the width of the wake decreases (Dargahi, 1989). In the case of a very shallow open channel flow, the combined actions of the bed

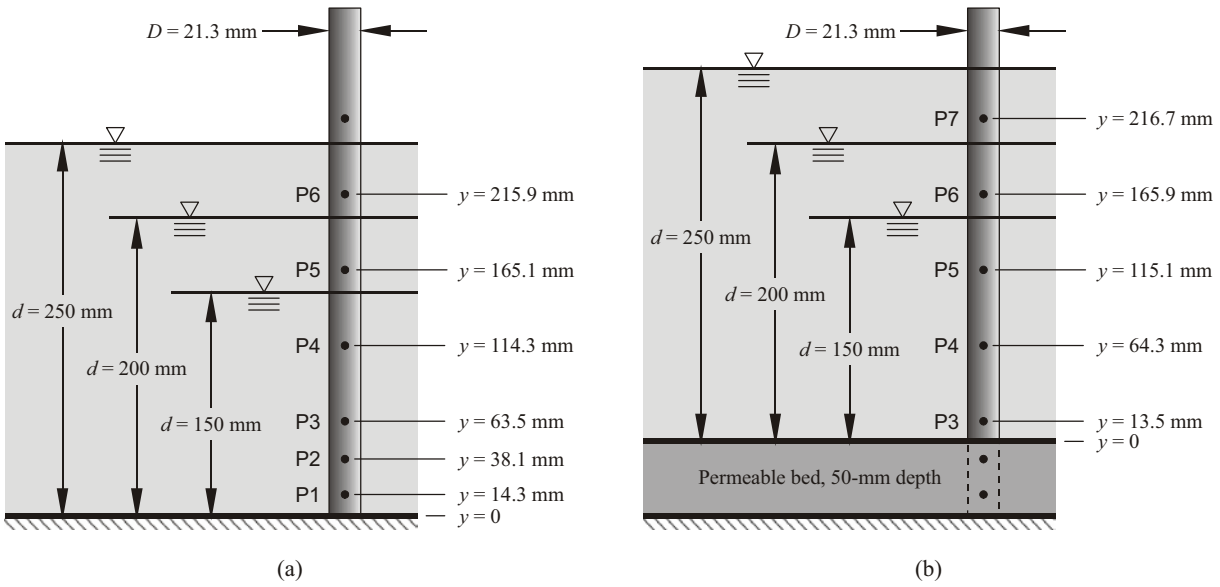

Fig. 3. Dye-injection port locations and channel depths: (a) impermeable beds; (b) permeable bed.

friction and the horseshoe vortex may stabilize the cylinder wake and annihilate the Kármán vortex street (Balachandar et al., 2000).

3. Experimental Set-Up and Instrumentation

Experiments were conducted in a 5-m long recirculating open channel hydraulic flume (Fig. 2(a)) with a square cross-section (0.5 × 0.5 m). Dye-injection flow visualization experiments with a circular cylinder were conducted on three different channel beds (smooth, rough impermeable, rough permeable) and at three different depths of flow (d = 150 mm, 200 mm, 250 mm). The rough bed experiments used 2-m long impermeable and permeable sand beds. The rough impermeable bed was made by applying a layer of sand grains to two sided-tape; similar tests have been carried out earlier in this laboratory with reliable results (Balachandar et al., 2001). For the experiments with a permeable bed, a raised, regular sand bed of 50-mm depth was constructed (Fig. 2(a)). A 0.3-m long ramp was erected before the leading edge of the sand bed to ensure a smooth transition. A sand grain with a D_{50} of 1.43 mm (the median diameter was determined from sieve analysis) was chosen for the experiments that allowed a visible amount of local scour without any general scour. In general, the flow was maintained such that the Reynolds shear stress was below the critical value for incipient motion. Experiments with similar velocities were also conducted on a smooth bed at the same location. One additional experiment was performed on the smooth bed at high velocity for comparison purposes. Previous experiments characterizing the turbulent boundary-layer-like flow on the smooth, rough impermeable, and rough permeable beds, using laser Doppler velocimetry (LDV), are reported by Rao (2003). Examples of the channel mean velocity profiles are shown in Fig. 2(b). In the present experiments, the maximum flow velocity, close to the free surface, ranged from U_e = 0.08–0.21 m/s. The longitudinal freestream turbulence intensity ranged from 0.5% near the free surface to 2.75% near the channel bed.

A hollow, smooth, stainless steel circular cylinder was used, with D = 21.3 mm and a height of 300 mm (which extends above the free surface), resulting in a solid blockage ratio of 4.26%. The Reynolds number ranged from Re_D = 1500–4400 based on the cylinder diameter, and from Re_H = 7,800–27,600 based on the channel hydraulic radius. The cylinder had seven pairs of dye-injection ports designated P1 through P7; see Fig. 3. The two ports comprising each pair were situated diametrically opposite to each other. Stainless steel tubes were welded internally to the ports and silicone tubing was used to connect these pipes to an acrylic manifold. The cylinder was centred between the channel walls at a distance of 1 m (47D) from the start of the test section bed (Fig. 2(a)).

Dye-injection flow visualization was used to study the flow around the cylinder. The cylinder

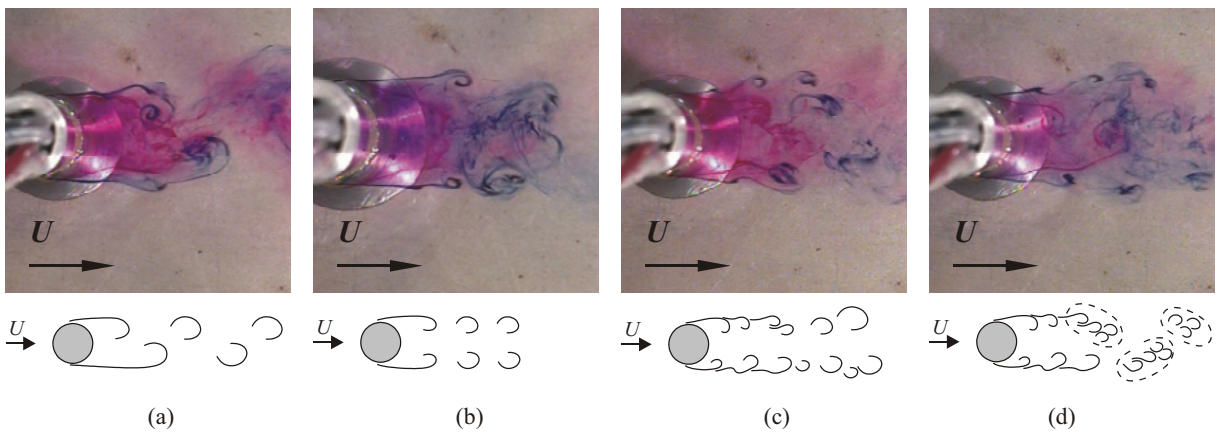

Fig. 4. Modes of vortex shedding and flow behaviour: (a) periodic, alternate Kármán vortex shedding; (b) symmetric vortex shedding; (c) irregular vortex shedding; (d) agglomeration process.

was oriented with the ports situated at ± 90° from the forward stagnation point, so the dye could be introduced into the separating shear layers developing from the cylinder. Water-soluble navy blue and red dyes were used, similar to Ramachandran (1999) and Balachandar et al. (2000). By changing the height of the dye reservoirs, and by adjusting flow valves, the dye flow rates were adjusted to match the local flow velocity. A Sony Digital Video Recorder DCR-TRV was installed above the flume to capture the top view of the flow. A Sony Hi-8 video camera was installed beside the flume to capture the side view of the flow. The videos were studied and images corresponding to each port location, that were representative of the flow behaviour, were selected.

4. Results and Discussion

The flow visualization results are divided into two parts, namely the (i) smooth bed experiments and the (ii) rough bed experiments (for both the impermeable and the permeable cases). For the smooth bed experiments, dyes of different colours were injected simultaneously at two different levels, to facilitate comparisons between the flow behaviour at different distances from the bed. Blue dye was injected from the topmost submerged port (closest to the free surface) and red dye was injected at the other pairs of ports below, sequentially at various distances from the bed.

In the present case of the wall-mounted cylinder in a shallow open channel flow, three different modes of vortex shedding were observed (Fig. 4). Apart from the conventional, periodic alternate Kármán vortex shedding (Fig. 4(a)), symmetric (Fig. 4(b)) and irregular (Fig. 4(c)) vortex shedding modes were observed. Other researchers (Dargahi, 1989; Lin et al., 1995) have also reported different modes of vortex shedding in similar bluff-body flows. In a given experiment, with the velocity remaining unchanged, all three modes were observed and the modes were found to change intermittently from one type to the other. For the symmetric vortex shedding mode (Fig. 4(b)), vortices are shed simultaneously from both sides of the cylinder. For the irregular vortex shedding mode (Fig. 4(c)), there is no definite phase relationship or periodicity for vortex formation and shedding. The existence of these three modes may be attributed primarily to the effects of bed friction, which extend throughout the depth of flow in a shallow open channel. Previous studies of bluff bodies in shallow open channel flows have shown that the bed friction effects are particularly strong, and can either suppress Kármán vortex shedding or cause it to become intermittent (Balachandar et al., 1999, 2000). In these flows, bed friction acts to reduce the entrainment of surrounding fluid into the wake and the spread rate and width of the wake. The result is a weakened interaction between the separating shear layers and a stabilization of the wake, and hence the potential for different modes of vortex shedding to appear. Other factors that may combine to produce the different modes include: (i) the elevated freestream turbulence intensity in the open channel flow; (ii) the action of horseshoe vortex at the cylinder-bed junction, which undergoes quasi-periodic shedding (Dargahi, 1989); and (iii) the influence of the different cylinder end conditions (channel bed, free surface),

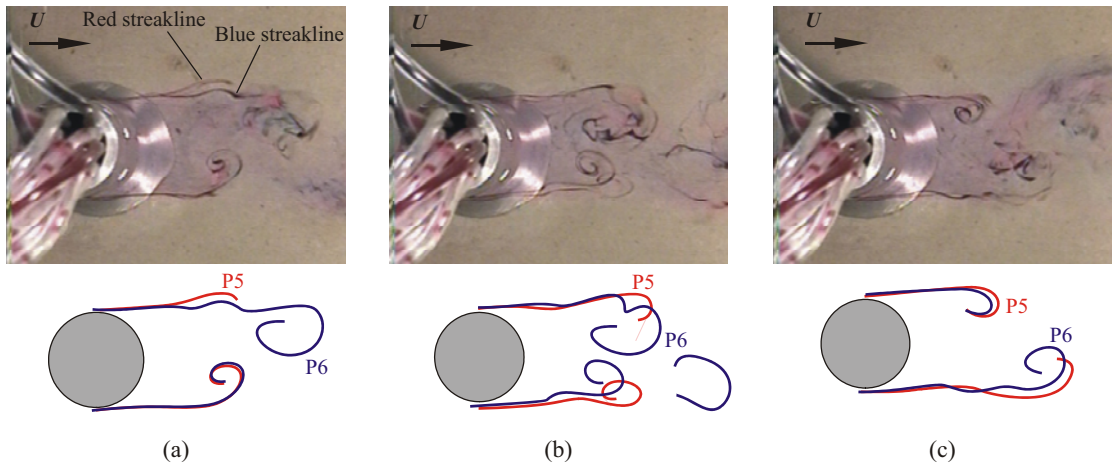

Fig. 5. Smooth bed, d = 250 mm, d/D = 11.7, Re_D = 2200, Re_H = 9600, blue dye from P6 (y/d = 0.86), red dye from P5 (y/d = 0.66): (a,b,c) alternate vortex shedding synchronized between P6 and P5.

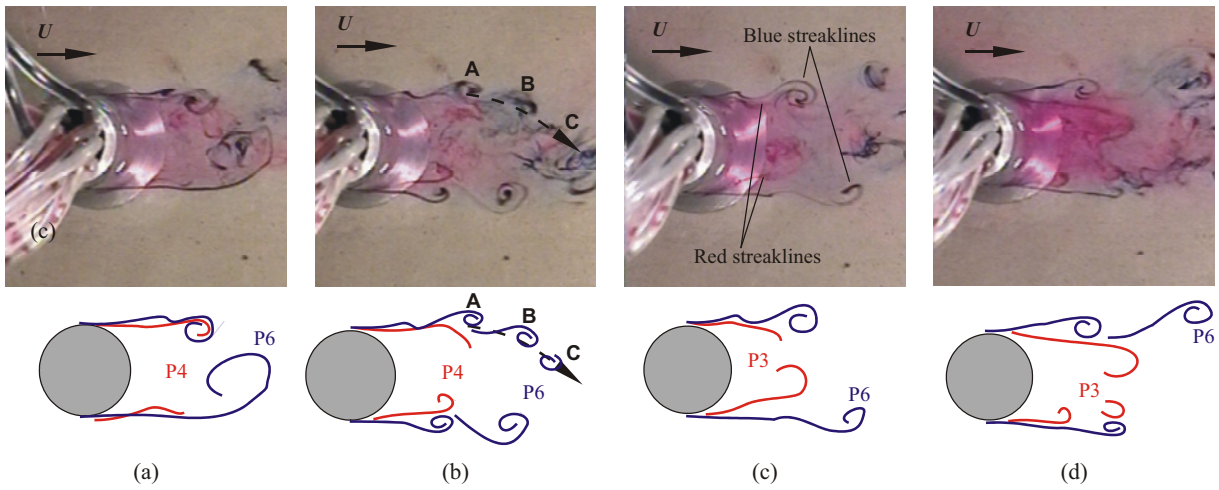

Fig. 6. Smooth bed, d = 250 mm, d/D = 11.7, Re_D = 2200, Re_H = 9600, blue dye from P6 (y/d = 0.86): (a) alternate vortex shedding synchronized between P6 and P4 (y/d = 0.46); (b) nearly symmetric vortex shedding and agglomeration, red dye from P3 (y/d = 0.25): (c) alternate vortex shedding from P6 and P3 but 180° out of phase; (d) irregular vortex formation from P6 and P3.

which can have a pronounced effect on the vortex shedding behaviour for cylinders of low aspect ratio (Williamson, 1996).

During the symmetric and irregular modes of vortex shedding (Figs. 4(b) and (c)), a fourth type of behaviour was observed that involved the agglomeration of several small vortices into larger, composite vortices (Fig. 4(d)). The composite vortices are convected into the intermediate wake, first from one side of the cylinder and then from the other, in an alternating fashion. The process acted to reorganize the flow, from symmetric or irregular shedding modes in the near-wake region, to an oscillatory behaviour similar to a Kármán vortex street in the intermediate wake. The process is similar to the coalescence or amalgamation of shear layer instability vortices into a forming Kármán vortex (Wei and Smith, 1986), but was generally a feature of the symmetric and irregular vortex shedding modes only. The agglomeration of small vortices into a composite vortex has also been observed by Freymuth (1985) and Sumner et al. (1999). The three modes of vortex shedding and the agglomeration mechanism (Fig. 4) were observed for all three channel beds (smooth, rough impermeable, and rough permeable) and at all three depths (d = 150 mm, 200 mm, and 250 mm).

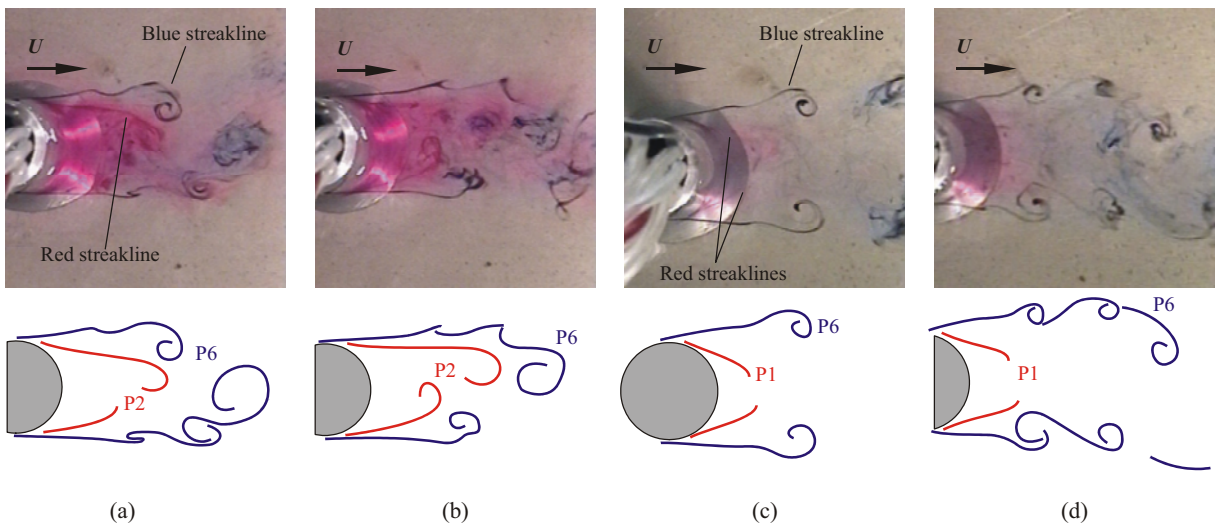

Fig. 7. Smooth bed, d = 250 mm, d/D = 11.7, Re_D = 2200, Re_H = 9600, blue dye from P6 (y/d = 0.86): (a) alternate vortex shedding from P6 and P2 (y/d = 0.15); (b) irregular vortex formation from P6, alternate, vortex shedding from P2; (c) symmetric vortex shedding from P6, red dye from P1 (y/d = 0.06); (d) agglomeration of vortices from P6.

4.1 Smooth Bed Tests

Figure 5 shows a set of flow visualization images for d = 250 mm. Blue dye was injected from the topmost submerged port P6 (y/d = 0.86, measured from the smooth bed) and red dye was injected first from the next lower port P5 (y/d = 0.66); it is sometimes difficult to distinguish between the red and blue dye streaklines, however, since the two lie one above the other, the near-wake width and the vortex formation length at both elevations are similar, and there is hardly any dispersion of the dye. Figure 5 shows examples of alternate vortex shedding, where it is seen that the vortex from one side of the lower port P5 is being released at the same time as the vortex from the same side of port P6, i.e. they are synchronized. Synchronization of vortex shedding along the axis or span of a cylinder is often expressed as a spanwise correlation length, which represents the distance along the cylinder axis over which the behaviour of the separated shear layers and vortex shedding remains similar. For an infinite cylinder in low-turbulence flow, correlation lengths are on the order of 2 to 3 diameters (Sumer and Fredsoe, 1997; Szepessy and Bearman, 1992; Szepessy, 1994). The distance between ports P6 and P5 is 2.3 diameters, and therefore synchronization would be expected, even at the elevated freestream turbulence intensity present in the open channel flow, which tends to lower the correlation length (Szepessy and Bearman, 1992).

Also for d = 250 mm, Figs. 6(a) and (b) show red dye being injected through the next lower port P4 (y/d = 0.46), while blue dye continues to be injected at P6 (y/d = 0.86) closest to the free surface and farthest from the bed. Figure 6(a) shows that vortex shedding can remain synchronized between P6 and P4, although it is less apparent in the irregular vortex shedding mode illustrated in Fig. 6(b).

Figure 6(b) shows an example of the aforementioned agglomeration process (Fig. 4(d)), where a number of smaller vortices (denoted as A and B in Fig. 6(b)) is released from one side of the cylinder and tend to combine together into a composite or ensemble structure (denoted as C in Fig. 6(b)). Other researchers have also observed the shedding of a number of small vortices, and the subsequent amalgamation of the vortices into a larger structure. For example, Sumner et al. (1999) observed this same behaviour in a study of two side-by-side cylinders, where the two cylinders were in contact with one another. They report that the vortex shedding behaviour (or mode) was often symmetric or irregular, that the shear layers tended to break up into small concentrations of vorticity, and that these small vortices would then combine into a larger Kármán-like vortex that was subsequently shed. Also, Freymuth (1985) reports numerous examples of vortex formation and shedding behaviour, including vortex agglomeration and coalescence processes.

Again for d = 250 mm, Figs. 6(c) and (d) show the top view when the red dye is injected from a

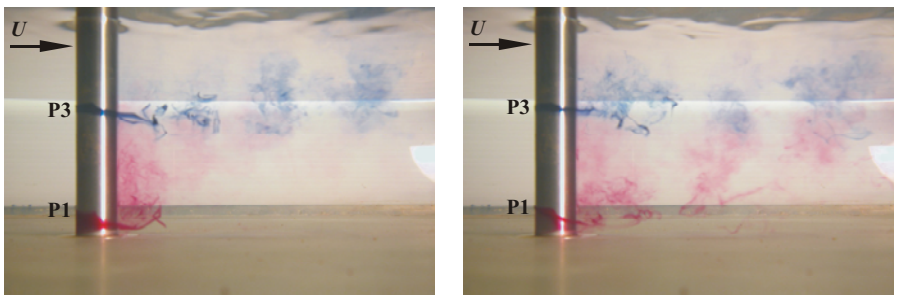

(a) (b)

Fig. 8. Smooth bed, side view, dye injected at the forward stagnation point at two levels: blue dye at mid-depth (P3), red dye near the bed (P1). (a) Red dye from P1 shows the horseshoe vortex moving upwards from the bed and interacting with vortex shedding at mid-depth (shown by blue dye from P3). (b) Red dye from P1 now shows vortex shedding similar to what is observed by blue dye from P3.

lower port, P3 ($y/d = 0.25$). With this increase in distance between the two ports, P3 and P6, vortex shedding is no longer synchronized. In Fig. 6(c), the vortices from the two ports are approximately 180° out of phase, i.e. while the vortex from the top port P6 is being shed from the one side, the vortex the lower port P3 is being shed from the opposite side. Other features noticed at the lower port P3, closer to the channel bed, are greater dispersion of the red dye, a smaller near-wake width, and a smaller vortex formation length. Fig. 6(d) shows the irregular vortex shedding mode at both ports P3 and P6, which continues to be observed along with the other modes of vortex shedding.

A closer look at Figs. 6(b) and (c) reveals a waviness in the shear layers emanating from the sides of the cylinder; the waviness is particularly evident for the blue dye streaklines emanating from P6. The waviness suggests that the shear layers experience some sort of "instability" (possibly a Kelvin-Helmholtz instability), characterized by small-scale fluctuations or movement of the shear layers and the appearance of small vortical structures or undulations within the shear layers.

Figure 7 shows the red dye being injected through the two lowermost ports, those closest to the channel bed, P2 ($y/d = 0.15$) and P1 ($y/d = 0.06$); the blue dye continues to be injected from port P6 ($y/d = 0.86$) closest to the free surface. The three modes of vortex shedding continue to be observed closer to the channel bed, with examples of alternate vortex shedding from P2 in Figs. 7(a) and (b) and symmetric shedding from P1 in Fig. 7(c), however, the increased level of dispersion of the red dye makes these modes more difficult to discern. In studying several such images, it is important to recognize that the red dye from the lower ports is generally diffused throughout the imaging plane. When viewed simultaneously from the top and the side (using both video cameras), this behaviour was attributed to the horseshoe vortex dispersing the dye in the vertical and horizontal directions. This phenomenon was seen when the dye was injected from the ports near the channel bed, where often the shear layer was not clearly discernable, whereas at distances away from the bed the shear layer was clearly visible and the dispersion was also reduced.

An example of the influence of the horseshoe vortex is shown in Fig. 8, where the flow is now viewed from the side and dye is being injected from the forward stagnation point only (the cylinder has been rotated 90°). In Fig. 8(a), red dye introduced near the channel bed at P1 enters the horseshoe vortex. Blue dye introduced from P3 at mid-depth reveals alternate vortex shedding, as seen by the alternating concentrations of blue dye with clear water in the wake. In the near-wake region, the horseshoe vortex rolls upward and interacts with vortex shedding at mid-depth. In Fig. 8(b), however, the horseshoe vortex structure has been shed and red dye streaklines from P1 near the channel bed indicate vortex shedding behaviour. The vortex shedding is shown, similar to Fig. 8(a), by alternating concentrations of red dye and clear water. Similar vortex shedding behaviour is observed in Fig. 8(b) at mid-depth (from blue dye injected from P3), however, the wake structure near the channel bed (captured by the red dye) lags that at mid-depth (captured by the blue dye).

It is also apparent from Fig. 7 that the vortex formation length and the near-wake width become significantly smaller closer to the channel bed; this is particularly evident at P1 ($y/d = 0.06$) shown in Figs. 7(c) and (d). Shear layer instabilities continue to be observed. Based on conclusions drawn from studying a large number of images it was noticed that for a given depth and flow

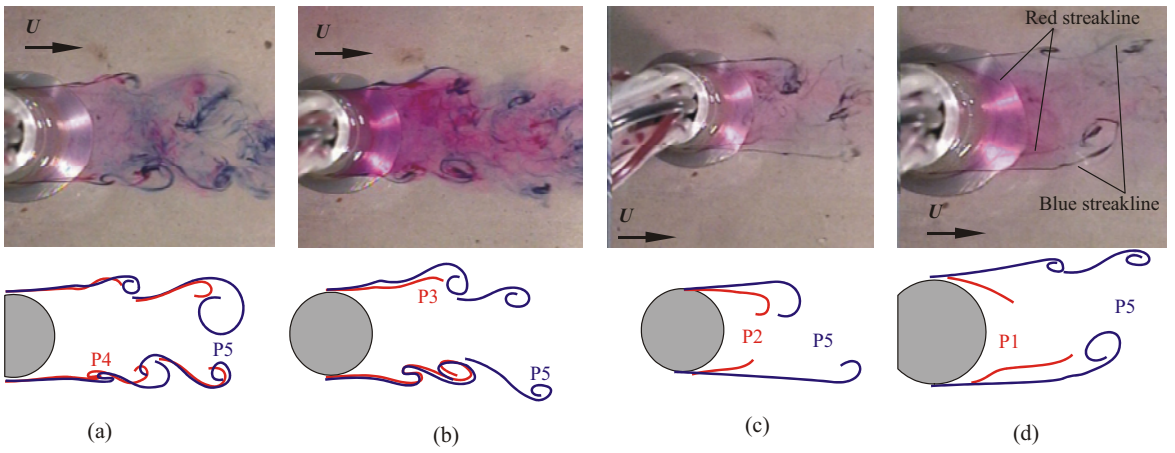

Fig. 9. Smooth bed, d = 200 mm, d/D = 9.4, Re_D = 2400, Re_H = 12,600, blue dye from P5 (y/d = 0.83): (a) red dye from P4 (y/d = 0.57), synchronized irregular vortex shedding at P5 and P4, agglomeration; (b) red dye from P3 (y/d = 0.42), mostly synchronized irregular shedding at P5 and P3; (c) red dye from P2 (y/d = 0.19), unsynchronized alternate vortex shedding from P5 and P2; (d) red dye from P1 (y/d = 0.07).

conditions, the distance between the dye ports decides the level of synchronization, if any. Despite the different modes of vortex shedding (alternate, symmetric, and irregular) observed in the near-wake region of the cylinder, the familiar undulating or oscillatory form of a Kármán vortex street was clearly recognizable in the intermediate wake, as mentioned above.

At a lower flow depth of d = 200 mm, where the topmost submerged port is P5 (y/d = 0.83), similar fluid-structure interaction occurs, see Fig. 9. The three modes of vortex shedding, the agglomeration process, and the spanwise synchronization of vortex shedding behaviour between adjacent ports, see Figs. 9(a) and (b), continue to be observed. When dye is injected closer to channel bed, again there is observed a narrowing of the near-wake region and a reduction in the vortex formation length, see Figs. 9(c) and (d). The main differences at the lower depths of d = 150 and 200 mm are related to the free surface, which was more disturbed when compared to d = 250 mm; the dispersion of the dye, which increased for both the blue and red dyes and at all ports; and the behaviour of the shear layers, which tended to exhibit more instabilities. It was also noted (from the side view) that the shear layers undergo larger-scale vertical oscillations, which are distinct from the smaller-scale shear layer "instability" behaviour described earlier (in the context of the top view). These vertical oscillations become increasingly greater at the lower depths of flow.

At all three depths of flow, on comparing the flow of the blue and red dyes from the topmost pair of ports (those pairs closest to the free surface, corresponding to $y/d > 0.42$), it is observed that the streaklines from the topmost two ports are synchronized. Also, the vortex formation lengths and near-wake widths are similar for a spanwise correlation length of less than 20%. Moreover, it is also seen that the level of dye dispersion and vertical oscillation of the shear layers increase steadily when moving closer to the channel bed and to lower depths. With increasing distance from the bed, the shear layer instabilities became weaker and the vortex formation length and the near-wake width both increase. These effects are caused by influence of the horseshoe vortex. Although the physical size of the horseshoe vortex is a function of d/D, the effects of the horseshoe vortex on the rest of the flow field will be more pronounced closer to the bed and will influence a greater proportion of the channel depth (or cylinder height) when the channel depth is shallower.

To better understand the agglomeration process (Fig. 4(d)), the flow at d = 150 mm and U_e = 0.1 m/s was captured with a high-speed camera (1020-Hz framing rate); see Figs.10 and 11. In Fig. 10(a), at time $t = t_o$, there are two vortices, designated A and B, where A is closer to the cylinder and is attached to the separating shear layer. In successive images, Figs. 10(b) and (c), vortex A convects towards vortex B, and finally the two agglomerate to form the composite or ensemble vortex structure C (Fig. 10(d)). Figure 11 shows a typical agglomerated ensemble C, which convects and grows in successive images. It is important to recognize the individual vortices forming the ensemble

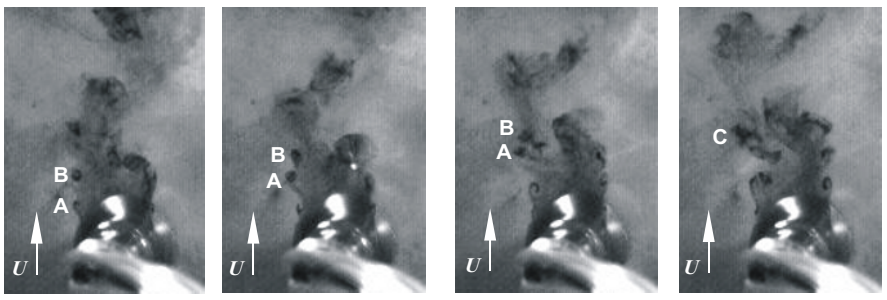

(a) $t = t_o$ (b) $t = t_o + 0.1$ s (c) $t = t_o + 0.2$ s (d) $t = t_o + 0.3$ s

Fig. 10. High-speed flow visualization, top view, smooth bed, d = 150 mm, Re_D = 2200, Re_H = 12,900, showing the agglomeration process: (a) vortices A and B just after formation of vortex A, time $t = t_o$; (b) vortices A and B moving closer together, time $t = t_o + 0.1$ s; (c) release of vortices A and B, $t = t_o + 0.2$ s; (d) agglomeration of vortices A and B into composite vortex structure C, $t = t_o + 0.3$ s.

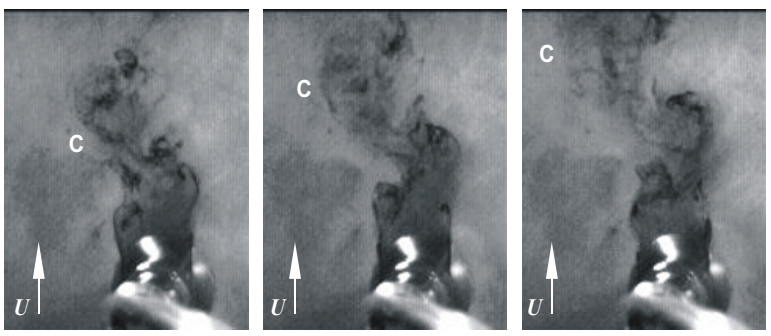

(a) $t = t_o$ (b) $t = t_o + 0.1$ s (c) $t = t_o + 0.2$ s

Fig. 11. Growth and convection of a composite or ensemble vortex, C (flow conditions as in Fig. 10).

are slowly losing identity and the large structure is shed downstream as part of an alternating vortex street. The alternate shedding nature of the intermediate wake is evident in Figs. 10(a) and 11(b), where the oscillatory appearance of a Kármán vortex street can be discerned.

4.2 Rough Bed Tests

Figure 12 shows a set of images for the rough impermeable bed, where the three modes of vortex shedding and the agglomeration process are again noted. For d = 250 mm on a smooth bed, as noted earlier, the shear layers near the free surface did not experience instabilities and there was no upward dispersion of the blue dye (Fig. 5(a), (b) and (c)). However, for the rough impermeable bed, Fig. 12(a), the effect of the horseshoe vortex is felt almost throughout the depth of flow (as recognized from the shear layer oscillations and instabilities and the dispersion of the dye). As noted in a previous study on open channel flow (Balachandar and Ramachandran, 1999), an increase in the skin-friction coefficient (amounting to an increase in the bed roughness) was found with decreasing depth of flow. To this end, visually comparing the flow past the cylinder at d = 150 mm on the smooth bed, with flow past the cylinder at d = 250 mm on the rough impermeable bed, the increase in dye dispersion is greater for the smooth-bed. In other words, a reduction in channel depth has a more pronounced effect on dye dispersion than a change from a smooth to a rough channel bed.

In the tests with the permeable bed the vortex shedding behaviour was similar to that observed for the smooth and rough impermeable beds with respect to the various phenomena discussed above. First, there was an increase in the vortex formation length and near-wake width with increased distance from the sand beds, at all three depths. Second, there was a decrease in vertical oscillations of the shear layers, and a decrease in dye dispersion, with increased distance from the bed. Asynchronous vertical oscillation of the shear layer was clearly evident (the independent oscillation of the shear layers at the two sides of the cylinder). It is interesting to note

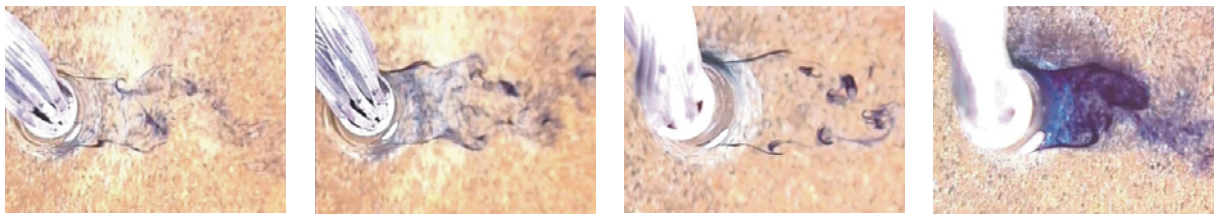

(a) (b) (c) (d)

Fig. 12. Rough impermeable bed, blue dye only, flow from left to right: (a) irregular vortex shedding, P5 (y/d = 0.66), d = 250 mm, d/D = 11.7, Re_D = 1600, Re_H = 9600; (b) symmetric vortex shedding, P5 (y/d = 0.66), d = 250 mm, d/D = 11.7, Re_D = 1600, Re_H = 9600; (c) agglomeration of shed vortices to form a larger composite or ensemble vortex, P4 (y/d = 0.46), d = 200 mm, d/D = 9.4, Re_D = 1500, Re_H = 7800; (d) alternate Kármán vortex shedding, P3 (y/d = 0.25), d = 200 mm, d/D = 9.4, Re_D = 1500, Re_H = 7800.

that for the rough permeable bed, however, the vertical oscillation of the shear layer is evident even at the topmost port (P7, Fig. 3(b)). Overall, the distinguishing characteristics of the permeable bed, compared to the impermeable bed, included further increases in the vertical oscillations of the shear layers, the level of the upward dispersion of the dye, and the distortion of the free surface.

5. Conclusions

The fluid-structure interaction for a circular cylinder mounted on a channel bed, in a shallow open channel flow, was studied with dye-injection flow visualization. For smooth, rough impermeable, and rough permeable beds, common flow behaviours attributed to interactions between the horseshoe vortex, shear layer dynamics, and vortex shedding, were observed. The flow was characterized by three different types or modes of vortex shedding behaviour: periodic alternate Kármán-type vortex shedding, symmetric vortex shedding, and irregular vortex shedding. The three modes were observed for all flow depths, at all elevations for a given depth, and for all three beds. The modes changed intermittently and randomly from one to another, but the dominant behaviour, i.e. the one that was observed most of the time, was the irregular shedding mode. Contrary to the observations of Dargahi (1989), the flow pattern changes did not appear to occur periodically at the Strouhal frequency. Given the predominance of the irregular vortex shedding behaviour, and the short duration of the various shedding modes, a repeatable value for the Strouhal frequency could not be discerned from frame-by-frame analysis of the flow visualization video. Some early experiments with a hot-film anemometer led to a similar conclusion, since the peak in the power spectrum of the velocity fluctuations was typically small and broad-banded.

In addition to the different modes of vortex shedding, the near-wake dynamics were characterized by the agglomeration of small vortices into larger ensembles of vortices, which were subsequently shed in an alternate fashion into the wake. Independent of the mode of vortex shedding, the intermediate wake of the cylinder was then characterized by an oscillatory flow pattern resembling a Kármán vortex street. Because of the rapid diffusion of dye, the individual vortices (which were, in most cases, ensembles or agglomerations of smaller vortices) comprising the street could not be discerned, however.

Oscillation of the shear layers in the cross-stream and vertical directions also was consistently observed. This activity was generally asynchronous, i.e. the motion of the shear layer on one side of the cylinder was typically independent of the shear layer from the other side. This oscillatory behaviour was accompanied by changes to the near-wake flow patterns and modes of vortex shedding, although a direct correspondence between oscillations and mode changes could not be established. The origin of the oscillations is related, in part, to the effects of the horseshoe vortex, and also the higher levels of freestream turbulence in the shallow open channel flow.

At a given depth, with increasing y/d from the bed, there was a decrease in the vertical oscillations of the shear layers, a decrease in the dye dispersion after vortex shedding, an increase in the width of the near-wake region, and an increase in the vortex formation length. As the depth of flow was reduced, there were increases in the level of upward dispersion of dye, the appearance of

shear layer instabilities, and the free surface disturbance (based on visual observation). These effects were caused, in part, by the horseshoe vortex, which occupies a greater proportion of the flow as the channel depth is reduced. Also, in a shallow open channel flow, the skin-friction and turbulence intensity are both increased compared to a deeper open channel flow (Balachandar et al., 1999). Because of the elevated turbulence intensity, the dispersion of the dye increases.

The added effects of bed roughness (compared to the smooth bed) were increased shear layer instability, shear layer oscillations, and upward dispersion of dye along the cylinder axis. The general features of the flow were otherwise similar for the smooth and rough beds. The effect of the permeable bed was a further increase, or intensification, of the general effects of roughness within the near wake. For the permeable bed, it was also noticed that the shear layer oscillations, the shear layer instabilities, and the dispersion of the dye in the upward direction, did not decrease as much with distance as in the case of a smooth bed. The flow visualization studies confirmed, in a qualitative manner, previous channel turbulent velocity measurements by Rao (2003), which showed that the effects of roughness are experienced almost throughout the channel depth.

Overall, the results show that the interaction between the horseshoe vortex and the Kármán vortices pervades throughout the depth. The non-uniform approach velocity profile, bed roughness, and permeability appear to enhance the influence of the horseshoe vortex throughout the channel depth and along the cylinder span. Near the channel bed, the horseshoe vortex causes a narrowing of the near-wake region and a reduction in the vortex formation length. Further away from the channel bed (and towards the free surface), the influence of the horseshoe vortex occurs at a distance further downstream from the cylinder base, resulting in a widening of the near-wake region and an increase in the vortex formation length. The effect and influence of the horseshoe vortex, therefore, decreases with distance from the bed. Despite the influence of the horseshoe vortex, and the highly three-dimensional character of the junction flow, alternate shedding of ensemble vortices remains a prominent flow feature.

Acknowledgments

Support from the Natural Sciences and Engineering Research Council of Canada (NSERC), and the assistance of D. Deutscher, D. Pavier, and Engineering Shops, are gratefully acknowledged.

References

Ahmed, F. and Rajaratnam, N., Flow Around Bridge Piers, ASCE Journal of Hydraulic Engineering, 124 (1998), 288-300.

Balachandar, R., Bergstrom, D. J., Tachie, M. F., and Ramachandran, S., Skin Friction Correlation in Open Channel Boundary Layers, ASME Journal of Fluids Engineering, 123 (2001), 953-956.

Balachandar, R. and Patel, V. C., Rough Wall Boundary Layers on Plates in Open Channels, ASCE Journal of Hydraulic Engineering, 128 (2002), 947-951.

Balachandar, R. and Ramachandran, S. S., Turbulent Boundary Layers in Low Reynolds Number Shallow Open Channel Flows, ASME Journal of Fluids Engineering, 121 (1999), 684-689.

Balachandar, R., Ramachandran, S., and Tachie, M. F., Characteristics of Shallow Turbulent Near Wakes at Low Reynolds Numbers, ASME Journal of Fluids Engineering, 122 (2000), 302-308.

Balachandar, R., Tachie, M. F., and Chu, V. H., Concentration Profiles in Shallow Turbulent Wakes, ASME Journal of Fluids Engineering, 121 (1999), 34-43.

Bearman, P. W. and Morel, T., Effect of Freestream Turbulence on the Flow around Bluff Bodies, Progress in Aerospace Sciences, 20 (1984), 97-123.

Bergstrom, D. J., Tachie, M. F., and Balachandar, R., Application of Power Laws to Low Reynolds Number Boundary Layers on Smooth and Rough Surfaces, Physics of Fluids, 13 (2001), 3277-3284.

Dargahi, B., The Turbulent Flow Field around a Circular Cylinder, Experiments in Fluids, 8 (1989), 1-12.

Dasgupta, A. and Paudyal, G. N., Characteristics of Free Surface Flow Over a Gravel Bed, ASCE Journal of Irrigation and Drainage Engineering, 111 (1985), 299-319.

Dey, S., Time-Variation of Scour in the Vicinity of Circular Piers, Proceedings of the Institution of Civil Engineers: Water, Maritime & Energy, 136 (1999), 67-75.

French, R. H., Open-Channel Hydraulics, (1985), McGraw Hill, New York.

Freymuth, P., The Vortex Patterns of Dynamic Separation: A Parametric Study and Comparative Study, Progress in Aerospace Sciences, 22 (1985), 161-208.

Grass, A. J., Structural Features of Turbulent Flow Over Smooth and Rough Boundaries, Journal of Fluid Mechanics, 50 (1971), 233-255.

Griffin, O. M., Vortex Shedding from Bluff Bodies in a Shear Flow: A Review, ASME Journal of Fluids Engineering, 107 (1985), 298-306.

Istiarto, I., and Graf, W. H., Experiments on Flow around a Circular Cylinder in a Scoured Channel Bed, International Journal of Sediment Research, 16 (2001), 431-444.

Kahraman, A., Sahin, B., and Rockwell, D., Control of Vortex Formation from a Vertical Cylinder in Shallow Water: Effect of Localized Roughness Elements, Experiments in Fluids, 33 (2002), 54-65.

Krogstad, P. and Antonia, R., Structure of Turbulent Boundary Layers on Smooth and Rough Walls, Journal of Fluid Mechanics, 277 (1994), 1-21.
Krogstad, P. A. and Antonia, R. A., Surface Roughness Effects in Turbulent Boundary Layers, Experiments in Fluids, 27 (1999), 450-460.
Lin, J. C., Towfighi, J., Rockwell, D., Instantaneous Structure of the Near-Wake of a Circular Cylinder: On the Effect of Reynolds Number, Journal of Fluids and Structures, 9 (1995), 409-418.
Mendoza, C. and Zhou, D., Effects of Porous Bed on Turbulent Stream Flow Above Bed, ASCE Journal of Hydraulic Engineering, 118 (1993), 1223-1240.
Nikora, V., Goring, D., McEwan, I., and Griffiths, G., Spatially Averaged Open-Channel Flow Over Rough Bed, ASCE Journal of Hydraulic Engineering, 127 (2001), 123-133.
Norberg, C., Interaction Between Free-Stream Turbulence and Vortex Shedding for a Single Tube in Cross-Flow, Journal of Wind Engineering and Industrial Aerodynamics, 23 (1986), 501-514.
Ramachandran, S. S., Bed Friction Effects in Low Reynolds Number Shallow Flows, M.Sc. Thesis, Department of Mechanical Engineering, University of Saskatchewan, Saskatoon, SK, Canada (1999).
Rao, S. K., Fluid-Structure Interactions Between a Circular Cylinder and a Channel Bed, M.Sc. Thesis, Department of Mechanical Engineering, University of Saskatchewan, Saskatoon, SK, Canada, (2003).
Rouland, A., Three-Dimensional Numerical Modeling of Flow Around a Bottom-Mounted Pile and its Application to Scour, Series Paper No. 74 (2000), Department of Hydrodynamics and Water Resources, Technical University of Denmark.
Simpson, R. L., Junction Flows, Annual Review of Fluid Mechanics, 33 (2001), 415-443.
Sumer, B. M. and Fredsoe, J., Hydrodynamics around Cylindrical Structures, (1997), World Scientific, Singapore.
Sumner, D., Wong, S. S. T., Price, S. J., and Païdoussis, M. P., Fluid Behaviour of Side-by-Side Circular Cylinders in Steady Cross-Flow, Journal of Fluids and Structures, 13 (1999), 309-388.
Szepessy, S., On the Spanwise Correlation of Vortex Shedding from a Circular Cylinder at High Subcritical Reynolds Number, Physics of Fluids, 6 (1994), 2400-2416.
Szepessy, S. and Bearman, P. W., Aspect Ratio and End Plate Effects on Vortex Shedding from a Circular Cylinder, Journal of Fluid Mechanics, 234 (1992), 191-217.
Tachie, M. F., Bergstrom, D. J., and Balachandar, R., Rough Wall Turbulent Boundary Layer in Shallow Open Channel Flow, ASME Journal of Fluids Engineering, 122 (2000), 1-9.
Wei, T. and Smith, C. R., Secondary Vortices in the Wake of Circular Cylinders, Journal of Fluid Mechanics 169 (1986), 513-533.
Williamson, C. H. K., Vortex Dynamics in the Cylinder Wake, Annual Review of Fluid Mechanics 28 (1996), 477-539.
Yulistiyanto, B., Zech, Y., and Graf, W. H., Flow Around a Cylinder: Shallow-Water Modeling with Diffusion-Dispersion, ASCE Journal of Hydraulic Engineering, 123 (1998), 419-429.
Zagni, A. F. E. and Smith, K. V. H., Channel Flow Over Permeable Bed of Graded Spheres, ASCE Journal of Hydraulic Division, 102 (1976), 207-222.
Zippe, H. J. and Graf, W. H., Turbulent Boundary-Layer Flow Over Permeable and Non-Permeable Rough Surfaces, Journal of Hydraulic Research, 21 (1983), 51-65.

Author Profile

Sridhar K. Rao: He is a Part-Time Professor at St. Clair College, Windsor, Ontario. He received his M.Sc. (2003) in Mechanical Engineering from the University of Saskatchewan.

David Sumner: He is an Associate Professor of Mechanical Engineering at the University of Saskatchewan. He received his Ph.D. in Mechanical Engineering from McGill University. His research interests are in the fields of bluff-body aerodynamics, fluid-structure interactions, and unsteady flows.

Ram Balachandar: He is Head of the Department and Professor of Civil and Environmental Engineering at the University of Windsor. He was formerly a Professor of Civil and Geological Engineering at the University of Saskatchewan. His research interests are in the fields of hydraulic engineering, rough wall boundary layers, and flow past bluff bodies.